MAGNETIC SEMICONDUCTORS

Magnetic semiconductors possess pronounced magnetic properties in addition to the traditional electronic and optical properties common to all semiconductors. Magnetic semiconductors contain transition-metal or rare-earth magnetic ions (such as iron, manganese, europium, or other magnetic ions) as at least one of their constituents. The presence of the magnetic ions enhances the magnetic susceptibility of the materials relative to their nonmagnetic counterparts, and in some cases these semiconductors can exhibit spontaneous magnetization in the absence of an externally applied magnetic field. The electronic and optical properties of magnetic semiconductors are usually more sensitive to magnetic fields than their nonmagnetic counterparts, displaying large magnetoresistance and magnetooptic effects in many cases. The optoelectronic properties can also show unusual physical behavior even in the absence of applied fields, such as large changes in the optical absorption or conductivity caused by changes in temperature, attributed to the effects of magnetic ordering.

Within the class of magnetic semiconductors are two principal subclasses of materials. These are the concentrated magnetic semiconductors (1) and the diluted magnetic semiconductors (2). In concentrated magnetic semiconductors the magnetic ion fills a sublattice of the crystal, as in the ferromagnetic binary compound semiconductor EuO. Diluted magnetic semiconductors can have continuously variable concentrations of magnetic ions, as in the alloy $Cd_{1-x}Mn_xTe$, for which the manganese concentration (denoted by x) can vary from the concentrated antiferromagnet MnTe to the nonmagnetic chalcogenide CdTe. A recent addition as a third subclass of magnetic semiconductors are heterogeneous magnetic semiconductors, in which magnetic precipitates are dispersed inside an otherwise nonmagnetic semiconductor host (3).

Magnetic semiconductors can exhibit ferromagnetic, antiferromagnetic, paramagnetic, or spin-glass behavior depending on their chemical constituents and concentrations and on the temperature. The diluted magnetic semiconductors may exhibit nearly all these properties within a single ternary compound, such as CdMnTe, by continuously tuning the magnetic ion concentration from the concentrated to the extremely diluted limit. For this reason, the diluted magnetic semiconductors have been the subject of extensive research.

MAGNETISM IN SEMICONDUCTORS

The properties of magnetic semiconductors are governed by the interactions of the magnetic ions with each other, called the ion–ion exchange interaction, and by the interactions of the free-carriers with the magnetic ions, called the carrier–ion exchange interaction. The ion–ion interaction governs the magnetic susceptibilities and the magnetic ordering of the magnetic semiconductors. The carrier–ion interaction governs the magnetotransport and magnetooptical properties that are unique to magnetic semiconductors.

Magnetization and Susceptibility

The strongest ferromagnetic behavior in semiconductors is observed among the concentrated magnetic semiconductors. Notable semiconductor ferromagnets are the chalcogenides of europium EuO and EuS, and the chromium chalcogenides $CdCr_2S_4$ and $CdCr_2Se_4$. The low-field static susceptibilities of these materials exhibit Curie–Weiss behavior at temperatures above the magnetic transition temperature

$$\chi = \frac{C}{T - T_c} \tag{1}$$

where C is the Curie constant and T_c is the Curie temperature. Below the phase transition to the ferromagnetic phase, these materials exhibit a spontaneous magnetization $M(T)$ that increases with decreasing temperature.

Antiferromagnetic behavior is common among other concentrated magnetic semiconductors, such as the other chalcogenides of europium EuTe and EuSe. The concentrated manganese chalcogenides MnO, MnS, MnSe, and MnTe are all antiferromagnetic, as are the diluted magnetic semiconductors derived from these. The static low-field susceptibility at high temperature obeys a Curie-Weiss law

$$\chi = \frac{C}{T - \theta} \tag{2}$$

with a negative Curie temperature θ. The susceptibility deviates from the Curie-Weiss law as the temperature approaches the Neel temperature T_N at which the ions order antiferromagnetically.

Extremely diluted magnetic semiconductors are approximately described as a paramagnetic phase for which the magnetic moments are uncoupled and are aligned by an externally applied magnetic field. The low-field high-temperature static magnetic susceptibility in this case takes on the simple Curie form.

In many of the diluted magnetic semiconductors a cusp is observed in the static susceptibility at a characteristic temperature T_g that is a function of the composition. This cusp in the susceptibility is accompanied by irreversible thermoremanence effects in the magnetization (4). These magnetic signatures may signal a phase transition from a paramagnetic phase to a low-temperature spin-glass phase. A spin glass consists of a configuration of spins that are frozen in random orientations. The spin glass exhibits no long-range order and is often caused by frustration of antiferromagnetic order.

Superparamagnetic behavior is characterized by a high-temperature static low-field susceptibility of the Curie form, but also exhibits irreversible thermoremanence in the magnetization. Superparamagnetism is caused by clusters of aligned spins. The macroscopic spin of the cluster is aligned by an applied magnetic field, contributing to the paramagnetic susceptibility. Superparamagnetism can occur in the case of ferromagnetic precipitates in nonmagnetic semiconductors (5). Although the irreversibility shows some similarity to spin-glass behavior, it can be described classically in terms of a spin-blocking temperature in which the individual magnetic fields of the isolated clusters mutually influence the alignment of the macroscopic moments of the other clusters.

Ion–Ion Exchange Interactions

Magnetic order in the absence of an applied magnetic field arises because of exchange interactions among the magnetic ions in the semiconductor. The simplest interaction Hamilto-

nian can be expressed as

$$H = -\frac{1}{2}\sum_{i,j} J(\mathbf{r}_i - \mathbf{r}_j)(\mathbf{S}_i \cdot \mathbf{S}_j) \tag{3}$$

where $\mathbf{S}_i$ is the spin of the ith magnetic ion, and $J(\mathbf{r}_i - \mathbf{r}_j)$ is the exchange integral between the spins on the ith and jth ions. For most magnetic semiconductors, the exchange occurs between pairs of magnetic ions that are too far apart for the direct exchange interaction to play a significant role. Therefore, the ions interact through the superexchange mechanism. Superexchange is an indirect exchange mechanism in which an intervening nonmagnetic ion (usually an anion) couples two magnetic ions. Superexchange most often produces antiferromagnetic coupling, but can also produce ferromagnetic ordering in some of the concentrated magnetic semiconductors.

Indirect exchange between magnetic ions, mediated through free carriers, can become important in degenerately doped semiconductors with high free-carrier concentrations. This interaction can lead to ferromagnetic ordering because the electron energy is lowered by spontaneous magnetization.

The superexchange and indirect exchange interactions lead to magnetic ordering of the magnetic ions at sufficiently low temperatures. Both ferromagnetic and antiferromagnetic order occur among the concentrated magnetic semiconductors, whereas the order in the diluted magnetic semiconductors is almost exclusively antiferromagnetic. Most transition temperatures are below room temperature, with exceptions observed for MnTe (323 K), NiO (520 K), and $CuFeS_2$ (825 K) among the antiferromagnets. The ferromagnet $CuCr_2Te_3I$ has a reported Curie temperature of 294 K (6).

Carrier–Ion Exchange Interactions

An important aspect of magnetic semiconductors is the effect of the magnetic ions on the electronic and optical properties of the free carriers. Although free carrier densities in nondegenerate semiconductors are too small for the electrons to effectively mediate indirect exchange between the magnetic ions, the free carriers themselves interact with the localized magnetic moments of the magnetic ions. The carrier exchange Hamiltonian takes on a form similar to Eq. (3):

$$H_{\mathrm{ex}} = -\sum_{R_i} J(\mathbf{r} - R_{\mathrm{i}})(\mathbf{S}_{\mathrm{i}} \cdot \boldsymbol{\sigma}) \tag{4}$$

where R_i is the location of the ith magnetic ion, $\mathbf{r}$ is the carrier position, and σ is the carrier spin. The carrier–ion exchange is a local interaction that depends on short-range magnetic order rather than on long-range order. This fact is most dramatically illustrated by the giant red shift in the absorption edge of ferromagnetic semiconductors even when the material is in the paramagnetic phase. The electron energy is reduced by the interaction with finite ferromagnetic clusters even though the macroscopic magnetization vanishes.

The localized moments of magnetic ions arise from localized d-shell or f-shell electrons, whereas the free-carrier states arise from s-shell and p-shell valence electrons. The carrier–ion exchange interaction is therefore often referred to as the sp-d or sp-f exchange mechanism. Two common contributions to the sp-d or sp-f exchange factor $J(\mathbf{r} - R_i)$ are a direct exchange interaction between the magnetic ion and the carrier and hybridization of the carrier wavefunction with the localized wavefunction. The direct exchange interaction is electrostatic in origin and leads to ferromagnetic interaction between the carrier and the ion. The contribution of hybridization to the exchange interaction is predominantly antiferromagnetic. It arises from the mixing of the sp wavefunctions of the anions with the localized d or f wavefunctions of the magnetic cations. Depending on the symmetries of the bands and of the localized wavefunctions for specific cases, either contribution can dominate.

Concentrated Magnetic Semiconductors

A distinction is made between those magnetic semiconductors that contain magnetic ions that fill a sublattice of the material, and those in which the magnetic sublattice is diluted by nonmagnetic ions. The former materials are called concentrated magnetic semiconductors and the latter are called diluted magnetic semiconductors.

Concentrated magnetic semiconductors share many of the optical and electronic properties in common with more traditional semiconductors, such silicon and germanium among the group IV elements, or GaAs and related III–V compounds. However, the magnetic semiconductors have significantly different crystal structure and carrier mobilities than the traditional semiconductors. Their magnetic properties and the effects of the magnetic structure on their electronic and optical structure have been studied extensively, although their development for electronic and optical applications remains at an early stage. The concentrated magnetic semiconductors are divided into two categories depending on whether they are antiferromagnets or ferromagnets at low temperature.

Antiferromagnetic Semiconductors

Many of the concentrated antiferromagnetic semiconductors have magnetic ions distributed on face-center cubic sublattices in the NaCl crystal structure. For this crystal structure, the three antiferromagnetic orderings that are most commonly observed are shown in Fig. 1. In type I antiferromagne-

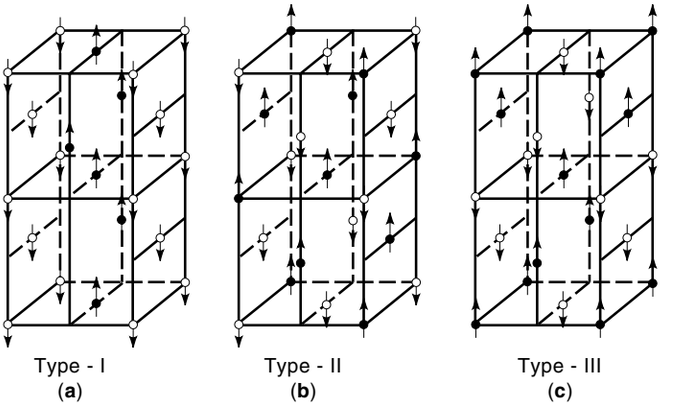

Figure 1. Three antiferromagnetic ordering in face-centered cubic magnetic sublattices, showing (a) type I with tetragonal symmetry, (b) type II with trigonal symmetry, and (c) type III with tetragonal symmetry.

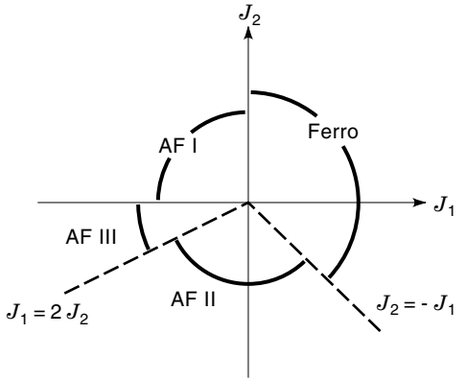

Figure 2. Magnetic phase diagram of the antiferromagnetic order depending on the nearest- and next-nearest-neighbor exchange integrals J_1 and J_2.

tism the magnetic ions form alternating planes of parallel spins perpendicular to a principal axis along ⟨100⟩, taking on tetragonal symmetry. In type II structures, which are the most common, the alternating planes of parallel spin occur orthogonally to the body diagonals along ⟨111⟩, taking on trigonal symmetry. In type III structures, the crystal structure including spin is again tetragonal with like spins distributed on a chalcopyrite sublattice. The stability of the different types of antiferromagnetic order are determined by the relative magnitudes and signs of the exchange constants J_1 and J_2 for nearest-neighbor and next-nearest-neighbor exchange interactions, respectively. The phase diagram is shown in Fig. 2 in the J_1 and J_2 plane for face-centered-cubic structures. Ferromagnetic order only occurs for positive nearest-neighbor exchange interaction and $J_1 > J_2$.

One of the most interesting and most exhaustively studied antiferromagnetic semiconductors is the rare-earth chalcogenide EuSe. In the absence of an applied magnetic field it changes from a paramagnet with decreasing temperature to an antiferromagnet at a Neel temperature of 4.6 K. However, it has a positive Curie temperature in the paramagnetic phase, indicating weak short-range ferromagnetic order. Upon the application of a magnetic field, the order changes from antiferromagnetic to ferrimagnet to ferromagnetic. This field-induced change in magnetic phase to ferromagnetic order is an example of a metamagnet. Other chalcogenides of europium, such as EuO and EuS are fully ferromagnetic. The magnetic semiconductor EuSe therefore rests on the border between antiferromagnetism and ferromagnetism. The remaining chalcogenide of europium, EuTe, behaves as an ordinary antiferromagnet with a Neel temperature of 9.58 K and a negative Curie temperature of −6 K. The exchange constants for the europium chalcogenides are given in Table 1

Table 1. Exchange Constants and Transition Temperatures for the Europium Chalcogenides

	θ (K)	$T_{c,N}$ (K)	J_1 (K)	J_2 (K)
EuO	79	69	0.606	0.119
EuS	18.7	16.6	0.228	−0.1.2
EuSe	8.5	4.6	0.073	−0.011
EuTe	−4.0	9.6	0.043	−0.15

From Wachter (7).

Table 2. Selected Antiferromagnetic Semiconductors

Material	T_N (K)	θ (K)
EuTe	9.58	−6
EuSe	4.6	9
Eu_3O_4	5.3	7
MnO	122	−610
α-MnS	154	−465
MnSe	173	−360
MnTe	323	−715
$MnTe_2$	80	−520
Gd_2Se_3	6	−10
NiO	520	−2600
CoO	291	−320
$LaMnO_3$	100	−500
$CuFeS_2$	825	
$CoCl_2$	25	−37
$NiCl_2$	50	−75
$ZnCr_2S_4$	18	18
$HgCr_2S_4$	60	137–142
$ZnCr_2Se_4$	20	115

From Nagev (1).

(7). The Neel and Curie temperatures for selected antiferromagnetic semiconductors are given in Table 2 (1).

Among the antiferromagnet chalcogenides are several oxides such as NiO and MnO. Many of the simple chalcogenides have NaCl crystal structures with the magnetic ions distributed on a face-centered cubic sublattice with type II antiferromagnetic order. The manganese chalcogenides are antiferromagnetic and constitute an important class of concentrated magnetic semiconductors because they represent the endpoints of the Mn-based diluted magnetic semiconductors, which are also antiferromagnetic.

Ferromagnetic Semiconductors

Ferromagnetic semiconductors have special properties not shared by the antiferromagnetic semiconductors, because the strength of the carrier–ion exchange depends on local order of the magnetic ion sublattice, which is opposite for the two cases. In ferromagnetic order, the magnetic moments align locally so that the contributions from each moment accumulates to produce large changes in the properties of the free carrier. For instance, the band-edge in ferromagnetic semiconductors experiences a pronounced red shift with decreasing temperature and shows the onset of spontaneous Faraday rotation below the Curie temperature. In addition, the sample resistivity shows a pronounced peak near the Curie temperature, and decreases significantly with increasing applied magnetic field. These effects are a consequence of the exchange interaction of the free carriers with the aligned moments of the magnetic ions.

Ferromagnetic semiconductors are not as ubiquitous as antiferromagnetic semiconductors and were discovered later. The first ferromagnetic semiconductor discovered was CrBr3 in 1960 (8), followed shortly by EuO and EuS (9). The Curie temperatures of these europium chalcogenides are 67 K and 16 K, respectively. More important for potential applications is the chromium spinel $CuCr_2Te_3I$, which has a Curie temperature near room temperature at 294 K (6). The Curie temper-

Table 3. Selected Ferromagnetic Semiconductors

Material	T_c (K)	Cell Moment (μ_B)
$CrBr_3$	37	3.85
EuO	66.8	6.8
EuS	16.3	6.87
EuB_6	8	
Eu_3P_2	25	6.8
Eu_3As_2	18	7.03
Eu_2SiO_4	5.4	
Eu_3SiO_5	9	7
Eu_3S_4	3.8	
Eu_4P_2S	24	
Eu_4P_2Se	22.5	
Eu_4As_2S	20	
$EuLiH_3$	38	
$CdCr_2S_4$	84.5–97	5.15–5.55
$CdCr_2Se_4$	130–142	5.4–6
$HgCr_2Se_4$	106–120	5.4–5.64
$CuCr_2Se_3Br$	274	5.25
$CuCr_2Te_3I$	294	4.10
$(CH_3NH_3)_2CuCl_2$	8.9	1
$KCrCl_4$	50–60	

From Nagev (1).

atures for selected ferromagnetic semiconductors are given in Table 3.

The giant red shift of the absorption edge with decreasing temperature is one of the consequences of the magnetic order in ferromagnetic semiconductors and is an effect that is unique to the magnetic semiconductors with no analog among ferromagnetic metals. This shift begins even in the paramagnetic phase in response to the formation of finite clusters of ferromagnetic spin alignment with which the free carriers interact through the *sp-d* or *sp-f* exchange mechanism. The red shift accelerates and is strongest near the Curie temperature, but continues for decreasing temperatures. The change of the energy gap as a function of temperature is shown in Fig. 3 for EuO and the spinel $HgCr_2Se_4$ (10,11). The red shift ceases when the temperature approaches $T = 0$ as the magnetization saturates. More complicated temperature dependences can also occur, including a blue shift in some cases, such as in $CdCr_2Se_4$.

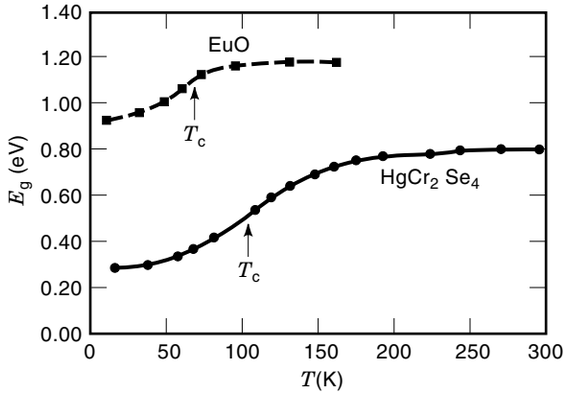

Figure 3. Red shift of the optical bandgap for EuO and $HgCr_2Se_4$ as a function of temperature (9,10). The Curie temperatures are indicated.

The resistance in nondegenerate *n*-type ferromagnetic semiconductors exhibits a strong peak at the Curie temperature. This effect is a consequence of the exchange-induced red shift of the conduction band-edge. For increasing temperatures below T_c, the conduction band-edge increases rapidly with respect to the Fermi level (pinned by extrinsic impurities), causing a decrease in the free-electron density. At temperatures larger than T_c, the thermal excitation of carriers from the impurity levels causes the usual increase in the carrier density that is observed for ordinary semiconductors.

Whereas nonmagnetic semiconductors usually have positive transverse-field magnetoresistance, ferromagnetic semiconductors show nearly isotropic negative magnetoresistance in which the resistance decreases under the application of a magnetic field. The drop in resistance has two origins: the reduction in magnetic fluctuations, and the change in carrier concentration with magnetic field. In the absence of a magnetic field, the local magnetization both above and below T_c fluctuates, causing carrier spin-scattering off the random orientations and magnitudes of the fluctuating moments. An applied magnetic field tends to orient the local moments, reducing the fluctuations and the scattering and increasing the conductivity of the material by increasing the carrier mobility. An applied magnetic field also shifts the conduction band-edge to lower energies closer to the impurity levels. This increases the conductivity of the material by increasing the carrier concentration. The magnitude of the magnetoresistance is largest for temperatures near T_c, where both the fluctuations and the shift of the band-edge are most sensitive to the applied field.

Faraday rotation of linearly polarized light in ferromagnetic semiconductors can attain record values under applied magnetic fields or at low temperatures. In EuS at 8 K in a field of 12 kOe the rotation can be as large as 10^6 deg/cm for some wavelengths of light (12). These values are larger than the largest values for Faraday rotation discovered in magnetic metals. Ferromagnetic semiconductors exhibit spontaneous Faraday rotation even in the absence of an applied magnetic field for temperatures below the Curie temperature, because the Faraday effect responds to the average macroscopic magnetization. The Faraday quality factor Q defines the rotation per decibel of light attenuation. In metals, because of the strong light attenuation at all wavelengths, the quality factor is typically less than 0.1 deg/dB. In the ferromagnetic semiconductors, because of the infrared transparency, the quality factor can be larger than 10^4 deg/dB, making these materials candidates for magnetooptical uses.

DILUTED MAGNETIC SEMICONDUCTORS

Diluted magnetic semiconductors are derived from the concentrated magnetic semiconductors by diluting the cation sublattice with nonmagnetic ions. This dilution process introduces alloy disorder within the sublattice, affecting the interactions by removing nearest- and farther-neighbor exchange interactions with increasing dilution. The dilution therefore changes the magnetic properties of the materials, such as magnetization and the transition temperatures. The dilution also often causes a change in crystal symmetry with important consequences for optical and electronic properties, as well as for the magnetic order.

Diluted magnetic semiconductors are important because the dilution process makes it possible to tune the magnetic properties of these materials to test theories of magnetic mechanisms in semiconductors. They are also important because they represent a means of introducing a magnetic dimension to technologically important nonmagnetic semiconductors. In the extreme dilute limit, diluted magnetic semiconductors may be viewed as being based on a nonmagnetic host to which magnetic cations are added. These semiconductors are sometimes referred to as semimagnetic semiconductors.

II–VI Based Diluted Magnetic Semiconductors

The best-studied examples of diluted magnetic semiconductors are the group II–VI semiconductors, in which a fraction x of the group II sublattice sites are replaced by magnetic ions. This class of diluted magnetic semiconductor is technologically important because the II–VI semiconductors are one of the classical semiconductor groups that are candidates for electronic and optoelectronic applications.

The structural properties of diluted magnetic semiconductors are controlled by the concentration of magnetic ions. The nonmagnetic II–VI semiconductors have tetrahedral coordination based on the sp^3 hybrid bond. They take on cubic zinc-blende or hexagonal wurzite structure depending on their composition. In the cubic phase, the cations form a face-centered cubic sublattice. The most common diluted magnetic form of the II–VI semiconductors is based on the Mn^{2+} ion that has a half-filled d-shell with a total spin $S = 5/2$. Other magnetic cations are also used, such as Cr^{2+} ($S = 4\theta 2$), Fe^{2+} ($S = 4/2$) and Co^{2+} ($S = 3/2$). These diluted magnetic semiconductors have the chemical formula $C_{1-x}M_xA$, where C refers to cation, M refers to magnetic ion, and A refers to anion. Examples are $Cd_{1-x}Mn_xTe$ and $Zn_{1-x}Mn_xSe$ in which the fraction of cations replaced by magnetic cation is given by x.

Not all values of x lead to homogeneous crystal structures. For each of the original II–VI semiconductor hosts, there is a maximum value of x that is permissible for bulk growth. In some cases, the crystal structure changes from cubic to hexagonal with increasing x, up to a maximum allowable concentration before the hexagonal phase is no longer stable. This parameter space is shown for the manganese-based compound semiconductors in Fig. 4. It should be pointed out that these conditions are relaxed for nonequilibrium epitaxial growth.

In the extreme dilute limit, the diluted magnetic semiconductors are paramagnetic and the low-field and high-temperature magnetic susceptibilities exhibit Curie law dependence. The low-field susceptibility takes on the Curie form where the Curie constant is

$$C_0 = \frac{N_0(g_{\text{ion}}\mu_B)^2 S(S+1)}{3k_B}x \tag{5}$$

where S is the spin of the magnetic ion, g_{ion} is the g factor of the magnetic ion, and N_0 is the number density of cation sites. The Curie constant depends linearly on x in the dilute limit. In the paramagnetic phase in the range of higher concentration and higher temperatures, the low-field susceptibility converts to a Curie–Weiss form where the Curie temperature is

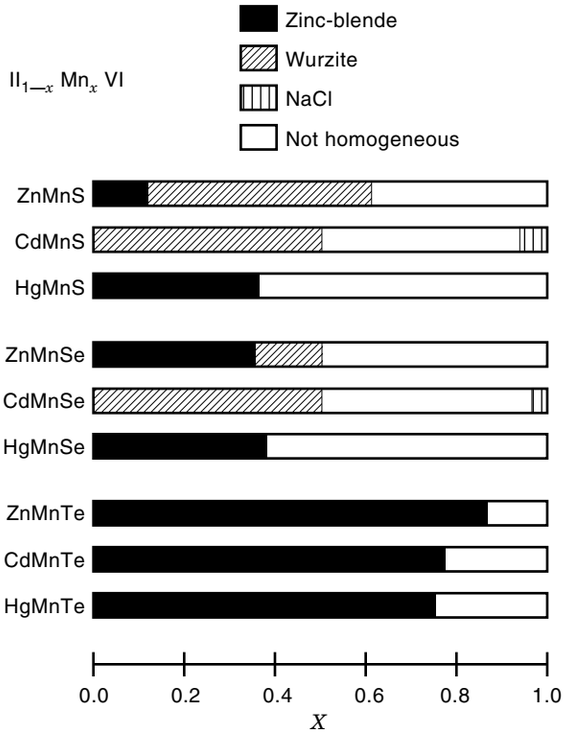

Figure 4. Composition ranges and crystal structures of the Mn-based group II–VI diluted magnetic semiconductors showing the range of homogeneous zinc-blende and wurzite structures. MnTe has a hexagonal NiAs crystal structure, whereas MnS and MnSe both have NaCl structures.

given by

$$\theta_0 = -\frac{2}{3}S(S+1)Z\frac{J}{k_B}x \tag{6}$$

which depends linearly on magnetic ion concentration in the dilute limit, and where J is the nearest-neighbor exchange constant, and Z is the number of nearest-neighbor cation sites ($Z = 12$ in zinc-blende and wurzite structures). The Curie temperature is negative for all the manganese-based II–VI diluted magnetic semiconductors, demonstrating that the exchange interaction is antiferromagnetic in this class of magnetic semiconductors. Measurements of the Curie temperature in principle provide a measure of the exchange interaction strength J, although other techniques give more accurate values, such as high-field magnetization, and neutron and Raman scattering. Values for the exchange constants for nearest-neighbor manganese–manganese pairs are given in Table 4 (13) for the manganese-based diluted magnetic semiconductors.

In the general case of arbitrary concentration and temperature, the magnetization can be expressed through the phenomenological expression

$$M = x_{\text{eff}}N_0 g_{\text{ion}}\mu_B S B_S\frac{g_{\text{ion}}\mu_B SH}{k_B T_{\text{eff}}} \tag{7}$$

where $B_s(y)$ is the Brillouin function and x_{eff} and T_{eff} are fittable parameters.

Table 4. Exchange Constants for Nearest-Neighbor Mn–Mn Pairs in Mn-Based Diluted Magnetic Semiconductors

Alloy	J (K)
ZnMnS	−16.1
ZnMnSe	−12.7
ZnMnTe	−9.7
CdMnS	−10.6
CdMnSe	−8.1
CdMnTe	−6.6
HgMnSe	−10.9
HgMnTe	−7.2

From Furdyna (13).

At temperatures below a characteristic value T_g that varies with composition the diluted magnetic semiconductors exhibit magnetic susceptibilities and irreversible phenomena that are consistent with the formation of a spin-glass phase. A spin glass is a random arrangement of spins that become frozen-in below the glass transition temperature T_g. The glass transition temperature varies between 0 K for the extreme dilute limit to 40 K for high concentration of magnetic ions. The variation of the glass transition temperature is shown in Fig. 5 for ZnMnTe and CdMnTe (14).

The *sp-d* exchange interaction between the free carriers and the localized moments of the magnetic ions produces large changes in the electronic energies of the free carriers under applied magnetic fields. The exchange interaction in Eq. (4) can be rewritten as

$$H_{ex} = \sigma_z \langle S_z \rangle x \sum_R J^{sp-d}(\mathbf{r} - R) \tag{8}$$

where S_i is replaced by the thermal average $\langle S_z \rangle$ for a field applied along the z axis. In addition, by explicitly including the magnetic ion concentration x, the sum is carried out over the full cation sublattice. With these approximations, the electron energies of the lth Landau level are

$$\begin{aligned} E_{l\uparrow} &= E_g + \left(l + \frac{1}{2}\right)\hbar\omega_c + \frac{1}{2}\left(g^*\mu_B H - N_0 \alpha x \langle S_z \rangle\right) \\ E_{l\downarrow} &= E_g + \left(l + \frac{1}{2}\right)\hbar\omega_c - \frac{1}{2}\left(g^*\mu_B H - N_0 \alpha x \langle S_z \rangle\right) \end{aligned} \tag{9}$$

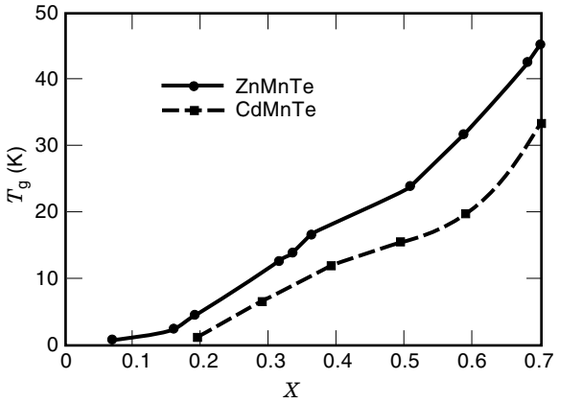

Figure 5. The spin-glass transition temperatures T_g as a function of composition for ZnMnTe and CdMnTe. Compiled in Furdyna and Samarth (14).

where E_g is the bandgap energy, ω_c is the cyclotron frequency, and g^* is the effective g factor of the conduction band electrons. The spin index refers to the electron spin orientation relative to the magnetic field. The exchange integral α for the s-like electrons of the conduction band is given by

$$\alpha = \langle S | J^{sp-d} | S \rangle \tag{10}$$

The electron energies can be expressed in terms of an effective g factor through

$$E_{l\pm} = E_g + \left(l + \frac{1}{2}\right)\hbar\omega_c \pm \frac{1}{2} g_{eff} \mu_B H, \tag{11}$$

where the effective g factor is

$$g_{eff} = g^* + \frac{\alpha M}{g_{ion}\mu_B^2 H} \tag{12}$$

which depends explicitly on the magnetization M. The effective g factor is temperature and concentration dependent, as well as field dependent, although in low-field and high-temperature situations, the ratio $M/H = \chi$ holds and is field-independent. The exchange contribution to the effective g-factor can exceed the band contribution by one to two orders of magnitude. The Zeeman splitting of the conduction band is therefore extremely large in the diluted magnetic semiconductors compared with the nonmagnetic materials.

The Zeeman splitting of the valence band is more complicated because it has Γ_8 symmetry with fourfold degeneracy. However, in this case it is possible to define an effective Luttinger parameter as

$$g_{eff} = \kappa - \frac{N_0 \beta x \langle S_z \rangle}{6\mu_B H} \tag{13}$$

where β is the exchange integral

$$\beta = \langle XYZ | J^{sp-d} | XYZ \rangle \tag{14}$$

Because of the p-symmetry of the valence band states, there is strong hybridization between the anion-like valence band and the d electron states of the magnetic cation, while the s symmetry of the conduction band states prevent significant hybridization with the localized d states. Therefore the β exchange constant is larger than α in the diluted magnetic semiconductors, producing larger Zeeman effects at the valence band edge. This result is opposite to the situation in the concentrated magnetic semiconductors in which the cationlike conduction band edge interacts most strongly with the magnetic cation.

The schematic splittings of the conduction and valence band edges are shown in Fig. 6 for wide-gap diluted magnetic semiconductors in which the exchange effects dominate over Landau and band g factor effects. The transitions are shown for specific light polarizations. For light propagating parallel to the magnetic field in the Faraday geometry the two eigenstates are right and left circularly polarized light, denoted by σ_+ and σ_-, respectively. For light propagating perpendicular to the magnetic field in the Voigt geometry, the eigenmodes are linearly polarized light denoted by π. The field dependence of the exciton transitions in ZnMnTe ($x = 0.05$) is shown in

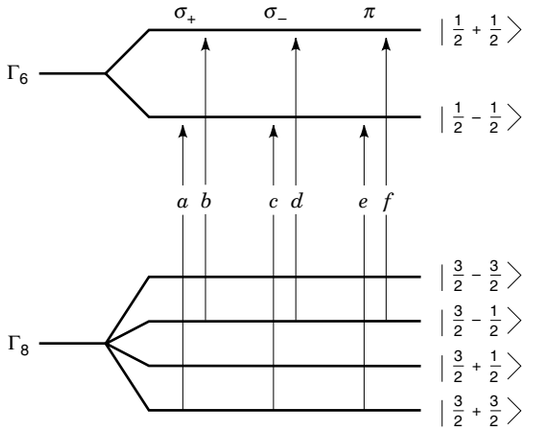

Figure 6. The symmetries and splittings of the direct interband Γ_8 to Γ_6 transitions for wide-gap diluted magnetic semiconductors. The allowed transitions for right and left circular polarization and linear polarization are shown.

Fig. 7 for circularly polarized light (15). Splittings as large as 100 meV in fields of 8 T occur at a temperature of $T = 1.4$ K in this wide-gap semiconductor. In contrast to the wide-gap diluted magnetic semiconductors, in narrow-gap or extremely dilute wide-gap diluted magnetic semiconductors the relative contributions of the exchange and band contributions to the spin splittings become comparable and the spin-state ordering changes sign.

The Faraday effect is the rotation of linearly polarized light that propagates parallel to an applied magnetic field. The rotation can be extremely large in the diluted magnetic semiconductors, and has been referred to as the Giant Faraday Effect. The rotation angle θ_F per crystal length L is given by

$$\frac{\theta_F}{L} = \frac{\sqrt{F_0}}{2\hbar c}\frac{\beta - \alpha}{g_{ion}\mu_B} M \frac{\hbar^2\omega^2}{(E_g^2 - \hbar^2\omega^2)^{3/2}} \tag{15}$$

where F_0 is a constant (16). The rotation per unit length per unit field strength is expressed through the Verdet constant.

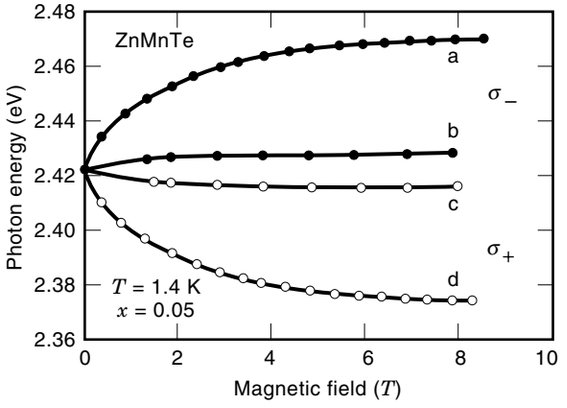

Figure 7. Energies of the a, b, c, and d transitions of Fig. 6 for ZnMnTe ($x = 0.05$) at 1.4 K in a magnetic field. From Aggarwall et al. (15).

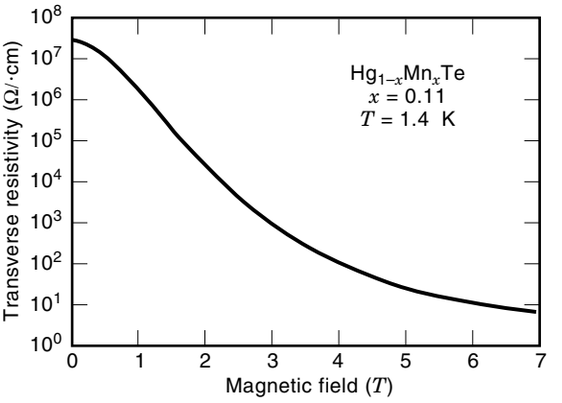

Figure 8. Giant transverse magnetoresistance in HgMnTe for $x = 0.11$ at $T = 1.4$ K. From Wojtowicz and Mycielski (17).

The Verdet constant for $Cd_{0.998}Mn_{0.002}Te$ can be as large as 3000 deg/cm · T for photon energies near the bandgap at a temperature near of 4 K (16).

The diluted magnetic semiconductors exhibit interesting magneto transport effects in addition to their magnetooptical effects. Narrow-gap diluted magnetic semiconductors, such as p-type HgMnTe, have giant negative magnetoresistance at low temperature. The transverse magnetoresistivity in $Hg_{0.89}Mn_{0.11}Te$ is shown in Fig. 8 at a temperature of $T = 1.4$ K (17). The resistivity decreases from $10^7\ \Omega \cdot$ cm in a zero-field to 10 $\Omega \cdot$ cm at 7 T. The giant magnetoresistance makes these materials candidates for use as recording heads for magnetic data memory. The increase in conductivity in an applied magnetic field is caused by the decrease of the acceptor binding energy combined with field-dependent changes in the defect wavefunction that produce anisotropic conductivity. Wider gap n-type CdMnSe also shows a negative magnetoresistance that has been attributed to magnetic polaron effects of the electrons.

A new direction in the optical studies of diluted magnetic semiconductors is the combination of the magnetooptic properties with photorefractive nonlinear optical effects. The interplay of the exciton-enhanced Faraday rotation with the polarization dependence of the electrooptic tensor of these materials produces interesting magnetic field dependence for photorefractive two-beam coupling (18). A more fundamental phenomenon in this respect is the connection between time-reversal symmetry and the quenching of phase-conjugate light by the application of a magnetic field (19).

MAGNETIC SEMICONDUCTOR HETEROSTRUCTURES

Semiconductors can be grown using epitaxial techniques such as by molecular beam epitaxy. This growth process opens up many possibilities for material growth and engineering. Molecular epitaxy is a layer-by-layer process that can provide layer-by-layer control to the crystal grower, making it possible to grow multiple layers of differing materials with monolayer accuracy. The diluted magnetic semiconductors can be grown by this technique, and interleaved between other magnetic layers or between nonmagnetic layers. The permutations of materials, layers, thicknesses and compositions in a

single heterostructure produces a nearly limitless variety of interesting processes.

The choice of substrate for epitaxial growth is an important feature of epitaxy of the diluted magnetic semiconductors. The choice is based on several factors, including cost and availability of the substrate material, as well as on the substrate lattice constant. For this reason, many epitaxial diluted magnetic semiconductor heterostructures are grown on GaAs substrates. Gallium arsenide is not ideally lattice-matched to any of the diluted magnetic semiconductors. The closest lattice match is for the alloy ZnMnSe, but even in this case a thick buffer layer is grown first on the GaAs to allow the lattice to relax to the correct value before the heterostructure is grown. Many of the strain relaxation defects are confined to the buffer layer, allowing relatively homogeneous growth of the heterostructures. However, many threading dislocations propagate up through the heterostructures, causing potential problems for applications.

Using lattice-mismatch epitaxy, forms of the concentrated magnetic semiconductors have been grown that do not exist in nature. For instance, natural MnSe occurs in the NaCl lattice structure, while $Zn_{1-x}Mn_xSe$ occurs in a zinc-blende structure only for x up to 35%, beyond which it transforms into a hexagonal phase which is limited to values $35\% < x < 50\%$. However, when grown epitaxially on a suitable substrate, thin films of MnSe have been grown in the zinc-blende phase (20).

An interesting feature of thin epitaxial layers of concentrated and diluted magnetic semiconductors is the absence of magnetic order. Bulk materials always exhibit antiferromagnetic order below a critical temperature, which is accompanied by a cusp in the linear magnetic susceptibility. In thin films of diluted magnetic semiconductors, on the other hand, the magnetic order is missing, and the magnetic properties are found to be paramagnetic (21).

A topic of keen interest in diluted magnetic semiconductors was the relatively large bandgap of the manganese-based zinc-blende compounds. The large bandgap makes these materials potential candidates for technologically important blue–green light emitting diodes and lasers. Optically pumped stimulated emission and laser oscillations in the blue–green spectral range were first observed in ZnSe/ZnMnSe multiple quantum wells operating at low temperature (22). Currently, the most attractive II–VI materials for blue lasers are sulfur-based injection lasers operating at room temperature without magnetic constituents (23).

One of the important aspects of epitaxial growth of diluted magnetic multilayer structures is the ability to interleave magnetic layers with nonmagnetic layers. Several different phenomena can occur in this situation. One example is the production of a spin superlattice by the application of a magnetic field. In the absence of a field, the superlattice potential is small, but the field causes a large Zeeman splitting in the magnetic layer that introduces a strong superlattice potential (24). Another example is the acquisition of magnetic properties by nonmagnetic layers, such as larger than usual Zeeman splitting of the excitons confined to the nonmagnetic layer. This occurs because the wavefunction penetrates into the magnetic layers containing magnetic ions.

Continuing interest in heteroepitaxy has led to more complex multilayer structures of diluted magnetic semiconductors, such as the growth of CdMgMnTe structures which can span the full visible range by varying the magnesium concentration, including the important blue spectral range (25). Nonequilibrium epitaxial growth techniques have made it possible to grow diluted magnetic III–V semiconductors, such as (In,Mn)As (26). Growth at low substrate temperatures (200°C) produced films that formed a homogeneous alloy, while higher growth temperatures (300°C) produced materials that had inclusions of ferromagnetic MnAs clusters. More recent work has extended the diluted magnetic III–V semiconductor materials to include (Ga,Mn)As (27) and (Ga,Mn)Sb (28), as well as superlattices of magnetic and nonmagnetic layers (29).

BIBLIOGRAPHY

1. E. L. Nagev, *Physics of Magnetic Semiconductors,* Moscow: Mir Publishers, 1983.
2. J. K. Furdyna and J. Kossut (eds.), *Diluted Magnetic Semiconductors,* Boston: Academic Press, 1988.
3. J. C. P. Chang et al., Precipitation in Fe- or Ni-implanted GaAs, *Appl. Phys. Lett.,* **65**: 2801, 1994.
4. S. B. Oseroff, Magnetic susceptibility and EPR measurements in concentrated spin-glasses: CdMnTe and CdMnSe, *Phys. Rev. B,* **25**: 6584, 1982.
5. T. M. Pekarek et al., Superparamagnetic behavior of Fe3GaAs precipitates in GaAs, *J. Magn. Magn. Mat.,* **168**: 1997.
6. S. Methfessel and D. Mattis, *Magnetic Semiconductors.* Berlin: Springer-Verlag, 1968.
7. P. Wachter, Europium chalcogenides: EuO, EuS, EuSe, EuTe. In *Handbook on the Physics and Chemistry of Rare Earths,* Vol. 2, Amsterdam: North-Holland Publishing, 1979, pp. 507–574.
8. I. Tsubokawa, On the magnetic properties of a CrBr3 single crystal. *J. Phys. Soc. Jpn.,* **15**: 1664, 1960.
9. B. Matthias, R. Bosorth, and J. van Vleck, Ferromagnetic interaction in EuO, *Phys. Rev. Lett.,* **7**: 160, 1961.
10. T. Arai et al., Magnetoabsorption in single-crystal HgCr2Se4, *J. Phys. Soc. Jpn.,* **34**: 68, 1973.
11. J. Schoenes and P. Wachter, Exchange optics in Gd-duped EuO, *Phys. Rev. B,* **9**: 3097, 1974.
12. J. Schoenes, P. Wachter, and F. Rys, Magneto-optic spectroscopy of EuS, *Sol. St. Commun.,* **15**: 1891, 1974.
13. J. K. Furdyna, Diluted magnetic semiconductors, *J. Appl. Phys.,* **64**: R29–R64, 1988.
14. J. K. Furdyna and N. Samarth, Magnetic properties of diluted magnetic semiconductors: a review, *J. Appl. Phys.,* **61**: 3526, 1987.
15. R. L. Aggarwal et al., Optical determination of the antiferromagnetic exchange constant between nearest-neighbor Mn ions in ZnMnTe, *Phys. Rev. B,* **34**: 5894, 1986.
16. D. U. Bartholomew, J. K. Furdyna, and A. K. Ramdas, Interband Faraday rotation in diluted magnetic semiconductors: $Zn_{1-x}Mn_xTe$ and $Cd_{1-x}Mn_xTe$, *Phys. Rev. B,* **34**: 6943, 1986.
17. T. Wojtowicz and A. Mycielski, Magnetic field induced nonmetal–metal transition in the open-gap HgMnTe, *Physica B,* **117** & **118**: 476, 1983.
18. R. S. Rana et al., Magnetophotorefractive effects in a diluted magnetic semiconductor, *Phys. Rev. B,* **49**: 7941, 1994.
19. R. S. Rana et al., Optical phase conjugation in a magnetic photorefractive semiconductor CdMnTe., *Opt. Lett.,* **20**: 1238, 1995.
20. L. A. Kolodziejski et al., Two-dimensional metastable magnetic semiconductor structures. *Appl. Phys. Lett.,* **48**: 1482, 1986.
21. S. Venugopalan et al., Raman scattering from molecular beam epitaxially grown superlattices of diluted magnetic semiconductors, *Appl. Phys. Lett.,* **45**: 974, 1984.

22. R. B. Bylsma et al., Stimulated emission and laser oscillations in ZnSe/ZnMnSe multiple quantum wells at 435 nm, *Appl. Phys. Lett.,* **47**: 1039, 1985.
23. R. L. Gunshor and A. V. Nurmikko, eds., II-VI blue/green light emitters: device physics and epitaxial growth, in *Semiconductors Semimetals,* vol. 44, San Diego, CA: Academic Press, 1997.
24. N. Dai et al., Spin superlattice formation in ZnSe/ZnMnSe multilayers, *Phys. Rev. Lett.,* **67**: 3824, 1991.
25. A. Waag et al., Growth of MgTe and CdMgTe thin films by molecular beam epitaxy, *J. Cryst. Growth,* **131**: 607, 1993.
26. H. Munekata et al., Diluted magnetic III–V semiconductor, *Phys. Rev. Lett.,* **63**: 1849, 1989.
27. F. Matsukura et al., Growth and properties of (Ga,Mn)As: a new III–V diluted magnetic semiconductor, *Appl. Surf. Sci.,* **113–114**: 178, 1996.
28. S. Basu and T. Adhikari, Variation of band gap with Mn concentration in GaMnSb—a new III–V diluted magnetic semiconductor, *Sol. State Commun.,* **95**: 53, 1995.
29. A. Shen et al., (Ga,Mn)As/GaAs diluted magnetic semiconductor superlattice structures prepared by molecular beam epitaxy, *Jpn. J. Appl. Phys. 2, Lett.,* **36**: L73, 1997.

DAVID D. NOLTE
Purdue University